
Zero-shot cross-modal transfer of Reinforcement Learning policies through a Global Workspace

Léopold Maytié

leopold.maytie@univ-tlse3.fr

CerCo, CNRS UMR5549

Artificial and Natural Intelligence Toulouse Institute
Université de Toulouse

Benjamin Devillers

benjamin.devillers@cnrs.fr

CerCo, CNRS UMR5549

Artificial and Natural Intelligence Toulouse Institute
Université de Toulouse

Alexandre Arnold

alexandre.arnold@airbus.com

Airbus AI Research

Rufin VanRullen

rufin.vanrullen@cnrs.fr

CerCo, CNRS UMR5549

Artificial and Natural Intelligence Toulouse Institute
Université de Toulouse

Abstract

Humans perceive the world through multiple senses, enabling them to create a comprehensive representation of their surroundings and to generalize information across domains. For instance, when a textual description of a scene is given, humans can mentally visualize it. In fields like robotics and Reinforcement Learning (RL), agents can also access information about the environment through multiple sensors; yet redundancy and complementarity between sensors is difficult to exploit as a source of robustness (e.g. against sensor failure) or generalization (e.g. transfer across domains). Prior research demonstrated that a robust and flexible multimodal representation can be efficiently constructed based on the cognitive science notion of a ‘Global Workspace’: a unique representation trained to combine information across modalities, and to broadcast its signal back to each modality. Here, we explore whether such a brain-inspired multimodal representation could be advantageous for RL agents. First, we train a ‘Global Workspace’ to exploit information collected about the environment via two input modalities (a visual input, or an attribute vector representing the state of the agent and/or its environment). Then, we train a RL agent policy using this frozen Global Workspace. In two distinct environments and tasks, our results reveal the model’s ability to perform zero-shot cross-modal transfer between input modalities, i.e. to apply to image inputs a policy previously trained on attribute vectors (and vice-versa), without additional training or fine-tuning. Variants and ablations of the full Global Workspace (including a CLIP-like multimodal representation trained via contrastive learning) did not display the same generalization abilities.

1 Introduction

Humans gather information from the world through multiple sources, leading to a rich and robust representation of their environment. Similarly, non-human agents should also learn to establish meaningful connections between information from different modalities. Such multimodal representation learning offers distinct advantages for decision-making and in particular in Reinforcement Learning. The benefits are evident when considering scenarios where one sensory input is noisy or unavailable. For instance, humans will be able to navigate in a room with subdued lighting where vision is compromised, as they can rely on other senses (hearing, touch...) to gather information

about their environment. In decision-making the ability to establish links between modalities allows more efficient problem-solving, because information from one sense can be leveraged to complete or verify data from another.

For these reasons, it seems advantageous to take inspiration from human multimodal integration and apply this to embodied RL agents, e.g. for robotics. A popular theory in cognitive science about how the brain handles multimodal information is the ‘Global Workspace Theory’ (Baars, 1988; Dehaene et al., 1998). According to this theory, different specialized modules compete to encode their information into a shared space called the Global Workspace. The shared representation is then broadcast back to all modules, leading to a unified interpretation of the environment. According to the theory, this last step corresponds to our inner experience. Importantly, compared to the unimodal representations in each specialized module, the shared representation enables multimodal *grounding* (Silberer & Lapata, 2012; Kiela & Clark, 2015; Pham et al., 2019), by linking objects and their properties across modalities. A deep learning-compatible adaptation of this theory has been proposed by VanRullen & Kanai (2021). The suggested model must meet several criteria (Fig 2): an alignment of the different latent representations and the capacity to translate from one modality to the other and to broadcast signals from the Global Workspace back to each module; ideally, the model can be trained in a semi-supervised setting with unsupervised cycle-consistency objectives. An initial implementation was reported in Devillers et al. (2023), and shown to provide reliable multimodal representations that could be leveraged advantageously for downstream classification tasks, all with minimal supervision.

In this work, we explore the use of a similar multimodal representation, inspired by the Global Workspace Theory, in the context of RL tasks. In particular, we show that this model is capable of zero-shot cross-modal policy transfer, in two different environments (see section 4), each with two modalities (vision: RGB images, attributes: a vector description of the agent and its environment). The first environment is called Factory, a virtual factory environment simulated in *Webots*; the second one is called Simple Shapes and made of simple geometric shapes.

2 Related Work

Representation learning for Reinforcement Learning is a vast and evolving field. Sutton & Barto (1998) already discussed the importance of compact representations for an RL agent. Deep Generative models, such as Variational Autoencoders (VAEs), have the capability to encode raw data into a compact and disentangled latent space. Pioneering work by Watter et al. (2015) and Finn et al. (2016) used this approach to encode representations for Reinforcement Learning, enhancing learning efficiency from high-resolution images. Compact representations are also crucial for algorithms relying on a World Model, such as the one introduced by Ha & Schmidhuber (2018). Further studies (Wang et al., 2023; Friede et al., 2023; Higgins et al., 2017) showed that learning disentangled environmental representations from a VAE enables agents to develop policies robust to some shifts in the original domain. Additionally, encoding observations in a well-structured space can be achieved through contrastive learning (Laskin et al., 2020; Du et al., 2021). With this method, Gupta et al. (2017) were even able to measure policy transfer between robots having different numbers of joints.

Representation learning has now extended to multimodal RL setups. Lee et al. (2019) use fusion mechanisms with Deep Neural Networks to handle multiple sources of observations. Singh et al. (2023) align visual latent representations with graphs using a contrastive loss, while Hafner et al. (2023) extend the work of Ha & Schmidhuber (2018) by using concatenated multimodal inputs for a world model. In a similar vein, Silva et al. (2020) extend DARLA’s work (Higgins et al., 2017) to two modalities: sound and vision. They employ a multimodal VAE (Yin et al., 2017) and align representations through an additional KL loss between the two modality-specific latent spaces. This AVAE model, like ours, allows zero-shot cross-modal policy transfer, e.g. training the policy with visual inputs and using audio inputs during inference. Thus, we will use this model as a baseline to compare against our approach.

Other multimodal representation learning models like CLIP (Radford et al., 2021) have been proposed to align two (or more) latent representations, and therefore to create a common space that can be used for downstream tasks. However such models require very large amounts of paired data between modalities to learn the aligned representation in a supervised way; in a robotic context, such paired data can be difficult to obtain. In addition, it has been shown that the contrastive alignment objective of CLIP tends to discard potentially important modality-specific information (Devillers et al., 2021). In our study, these two factors are investigated through ablation studies. First, we remove cycle-consistency objectives and train the model in a fully-supervised way. Second, we also remove the broadcast property (the ability to project global-workspace information back to each specialized module), leading to a contrastive-alignment version of our model similar to CLIP. As will be described below, both manipulations severely impair our model’s ability to transfer policies between modalities.

3 Problem Formulation

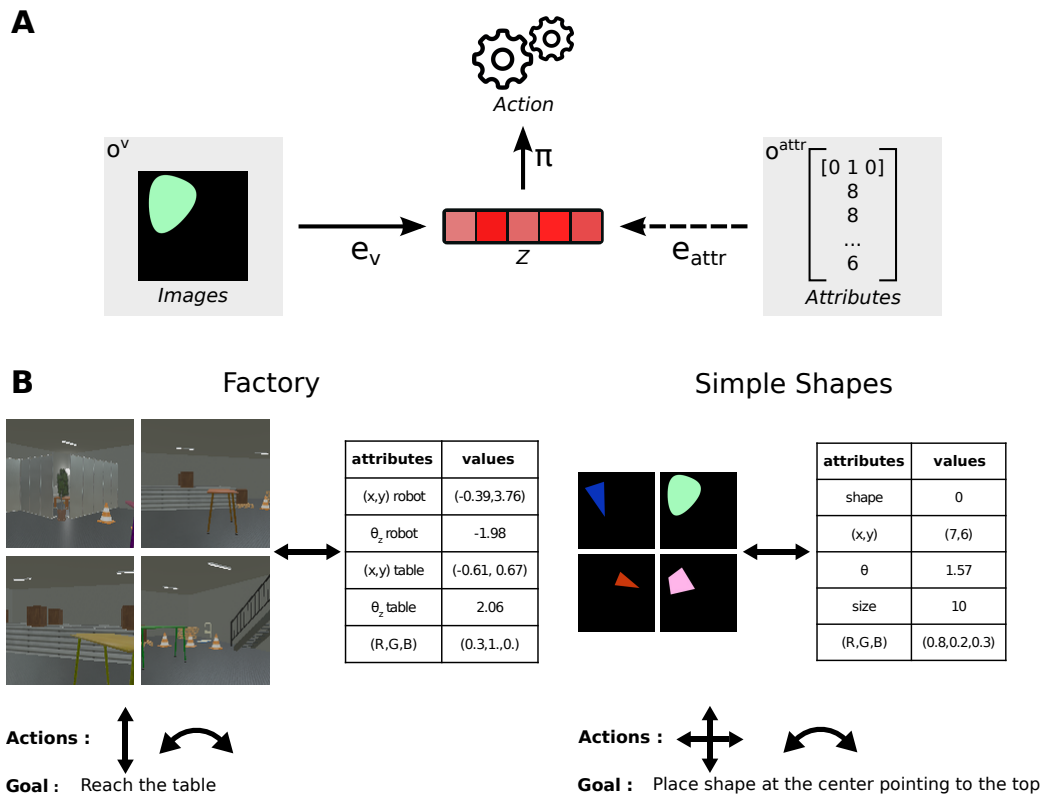


Figure 1: A: Overview of the general approach. Latent image or attribute representations can be encoded into a shared space $z \in \mathcal{Z}$ (the Global Workspace or GW) via encoders e_v and e_{attr} (respectively). The policy is trained (solid arrows) with observations from a given modality (here vision), with GW frozen. At inference time the policy can be tested with observations from a different modality (here attributes, dashed arrow); this is defined as *zero-shot cross-modal transfer*. B: Illustration of the two environments and tasks: *Factory* (left) and *Simple Shapes* (right). Example images and attributes are presented for each. For *Factory*, the agent must reach the table by rotating and moving forward or backward. For *Simple Shapes*, the agent must place the object at the center and pointing upwards, by moving to the right, left, top or down and rotating.

Let \mathcal{E} represent an environment, whose state at time t leads to an observation $o_t \in \mathcal{O}$, described as either a latent feature vector o_t^v computed from an RGB image, or an attribute vector o_t^{attr} . Based on these observations, the agent executes actions $a_t \in \mathcal{A}$ and receives a resulting reward r_{t+1} .

In this study, we first train a model to learn a representation $z_t \in \mathcal{Z}$ with two encoders $z_t^{attr} = e_{attr}(o_t^{attr})$ and $z_t^v = e_v(o_t^v)$. This step follows the approach previously described by Devillers et al. (2023), leading to a shared representation across modalities, i.e. a Global Workspace (GW). In a second step, with GW frozen, a policy π is trained to map GW-encoded observations from a specific training source $o \in \mathcal{O}^{train}$, with $train \in \{attr, v\}$, to actions $a \in \mathcal{A}$. During inference, the policy can potentially be transferred to another observation source \mathcal{O}^{test} , where $test \in \{attr, v\}, test \neq train$. The process is illustrated in Figure 1A, and the two training steps are further detailed below.

3.1 GW for multimodal Representation Learning

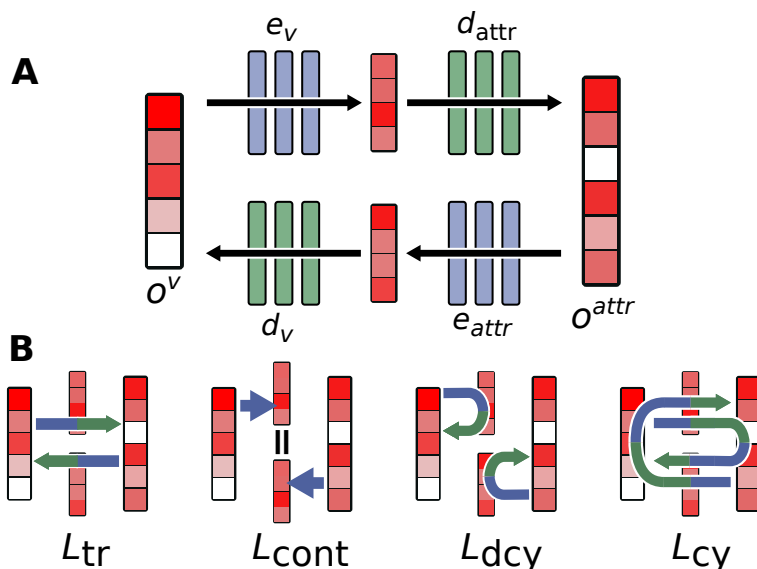


Figure 2: A: A generic view of the architecture of the Global Workspace where o^v and o^{attr} are encoded representations of the two modalities (vision, attributes). e_v , e_{attr} are feed-forward encoders into the GW representation, and d_v , d_{attr} are feed-forward decoders. Encoded representations of the two modalities $e_v(o^v)$ and $e_{attr}(o^{attr})$ are separate in the architecture, but can be aligned by virtue of the training objectives (illustrated in B), resulting in a shared GW. B: Illustration of the losses used during training of the encoders and decoders. The arrows represent the path used by the data to compute the losses. L_{tr} and L_{cont} are supervised losses for translation and contrastive alignment, respectively; they require paired training samples across the two modalities. In contrast, L_{dcyc} and L_{cyc} are self-supervised losses for demi-cycle and full-cycle consistency, respectively; they can be trained with unpaired samples from each modality.

We closely follow the training setup described in Devillers et al. (2023). That study evaluated the properties of a multimodal GW for low-resource semi-supervised training, and for downstream classification tasks; here, we are interested in applying such a system to train an RL agent. As in this previous study, we consider a setting where matched training data across modalities can be scarce or difficult to obtain, yet we have access to potentially large amounts of unimodal data (without matching labels in the other modality). Thus, we sample unimodal observations from two sets \mathcal{U}_{attr} and \mathcal{U}_v , and paired multimodal observations from the subset $\mathcal{M} = \mathcal{U}_{attr} \cap \mathcal{U}_v$, composed of observations that are paired across both unimodal sets.

As proposed in VanRullen & Kanai (2021); Devillers et al. (2023), we do not use raw images or attributes as inputs to the GW, but encoded representations into a unimodal latent space. For

images, we use a Variational Autoencoder (VAE), pretrained using the set \mathcal{U}_v ; for attributes, we simply normalize them between -1 and 1. Then, we train the GW itself, composed of a set of encoders for each modality $\{e_v, e_{attr}\}$ with their corresponding decoders $\{d_v, d_{attr}\}$ (Figure 2A). The role of the encoders is to project the two unimodal latent representations onto a shared one (the GW), where they should be aligned. The role of the decoders is to allow broadcast from GW back to the unimodal representations.

To train the network, four different losses are used (Devillers et al., 2023) (see Supplementary Material for losses definitions). The translation (L_{tr}) and contrastive alignment (L_{cont}) losses are supervised losses, optimized using the set \mathcal{M} . The full-cycle (L_{cy}) and demi-cycle (L_{dcy}) consistency losses are optimized using the full sets \mathcal{U}_{attr} and \mathcal{U}_v . Figure 2B illustrates how these losses are computed using the encoders and decoders of the GW. The total loss is a weighted sum of these four. Devillers et al. (2023) described implicit relations between the different losses, such that optimizing a subset of the losses can indirectly improve the others. By combining the four losses, the GW model optimizes the desired criteria of multimodal representation alignment and broadcast, while taking full advantage of unsupervised training data.

3.2 Policy Learning and cross-modal transfer

We use Proximal Policy Optimization (PPO), a widely adopted Reinforcement Learning algorithm introduced by Schulman et al. (2017). We also tested Advantage Actor Critic (A2C) introduced by Mnih et al. (2016), to validate our results on another algorithm (see Supplementary Materials).

To obtain an upper baseline for cross-modal transfer, we train two policies in a more classical way using only unimodal information (the two policies’ inputs are the unimodal representations of images o^v or attributes o^{attr}). This is compared with policies trained from GW-encoded representations of the observations, and tested either with observations from the same modality or from the opposite modality (i.e. zero-shot cross-modal transfer).

While our main test relies on a GW trained using all four losses (Figure 2B), we also trained policies from GW models optimized with fewer losses, serving as ablations of the full model. A GW trained in a fully supervised way (without the cycles losses L_{cy} and L_{dcy}) serves to assess the impact of semi-supervision, especially in low-data regimes (i.e., with few paired data in \mathcal{M}). We also trained a policy using a GW trained only with a contrastive loss L_{cont} . This ablation evaluates the impact of “broadcast” on the performance, and serves as a CLIP-like baseline because it is trained with the same alignment objective as CLIP (Radford et al., 2021). Finally, we compare our GW to an adaptation of the AVAE model used in Silva et al. (2020). We modify their visual VAE to match the architecture of our own visual VAE in each environment; we also replace their audio VAE by an attribute VAE, with an architecture adapted to match the dimensions of our attribute vectors (see Supplementary Material for architecture details). This transition from audio to attribute VAE also leads to a change in the reconstruction loss: we use the same attribute reconstruction loss as the one used in the GW (see Supplementary Material). Apart from these architectural changes, the AVAE model is trained in a supervised way (on the paired multimodal set \mathcal{M}), as described in the original paper (Silva et al., 2020).

For both environments, we evaluate policies based on multimodal systems (GW, GW without cycles, CLIP-like, AVAE) trained with two data regimes: either a large amount of matched data, $\mathcal{M} \equiv \mathcal{U}_{attr} \equiv \mathcal{U}_v$ (full data regime), or a small amount of paired data (low data regime: \mathcal{M} contains 1/4th of the full dataset for *Factory*, 1/100th of the full dataset for *Simple Shapes*). This assesses the impact of the unsupervised cycle-consistency losses, and the performance of fully supervised models in a low data regime.

4 Environments

We evaluate our approach on two different environments. Each one captures observations across the same two modalities: attributes describing the state of the agent, or an RGB image. The first

environment, called ‘Factory’ is a simulated factory shop floor in a robotic simulator: Webots. The second environment, named ‘Simple Shapes’ because it depicts a 2D shape on a dark background, is simulated directly using a Python-based Gymnasium environment (Towers et al., 2023).

4.1 Factory Environment

Simulated in Webots, this environment represents a factory-like shop floor with a Tiago robot and a table. The agent receives RGB images (128x128 pixels) from the robot’s viewpoint, or a set of seven attributes describing the robot and table states (Figure 1B). Robot state attributes include position (x_r, y_r) and rotation θ_r . Table state attributes include position (x_t, y_t) , rotation θ_t , and color h_t . The color is defined only by the Hue of HSV, with saturation and value set to 1 to retain high-contrast colors. The final attribute state vector concatenates attribute transformations: applying cosine and sine to angles, normalizing all attributes between -1 and 1, and decomposing the table’s Hue into a cosine-sine vector.

This environment displays an asymmetry between modalities, whereby images only provide partial information while attribute vectors offer exact information, even when the robot is not facing the table. At the beginning of each episode, table attributes are randomly sampled within their domains. The robot is placed near the center with a random angle, and the agent’s goal is for the robot to reach the table. The agent directly controls the position and rotation of the robot. The robot can move forward/backward and rotate (by a maximum of 5cm and $\frac{\pi}{16}$ radians during each step). Collisions with simulation objects (e.g. walls) lead to episode termination with a penalty of -10000 . At each timestep, the reward is equal to minus the distance between the robot and the table (in meters) minus $10 \times$ the angle (in radians) between the robot orientation and the robot-table vector, thus penalizing the agent for not facing the table. This approach aims to guide the robot to first locate the table by rotating and then move towards it, dividing the learning into two distinct goals and enhancing performance in scenarios where the agent relies solely on the robot’s vision. When the robot reaches the table, the episode concludes with no additional reward.

4.2 Simple Shapes Environment

The second environment, called ‘Simple Shapes’, was introduced in Devillers et al. (2023). The agent can receive two types of observations: 32×32 pixel RGB images of a 2D shape on a black background, or a set of eight attributes directly describing the environment’s state (Figure 1B). There are three different types of shapes, an egg-like shape, an isosceles triangle, and a diamond. They are represented by the variable $shape \in \{0, 1, 2\}$. The shape possesses a size $s \in [s_{min}, s_{max}]$, a position $(x, y) \in [\frac{s_{max}}{2}, 32 - \frac{s_{max}}{2}]^2$, a rotation $\theta \in [0, 2\pi[$ and an HSL color $(c_h, c_s, c_l) \in [0, 1]^2 \times [l_{min}, 1]$. The final attribute state vector concatenates transformations of these attributes: decomposing the rotation angle θ into $(c_\theta, s_\theta) = (\cos(\theta), \sin(\theta))$; translating HSL colors to the RGB domain, expressing the $shape$ variable as a one-hot vector of size three, and normalizing all the variables between -1 and 1.

At the beginning of each episode, attributes are randomly sampled within their respective domains. The agent’s goal is to move the shape to the center of the image at $(x, y) = (16, 16)$ and align it to point to the top, $\theta = 0$. Actions available to the agent include moving the shape by one pixel in cardinal directions (left, right, up, or down) and rotating the shape by an angle of $\frac{\pi}{32}$ clockwise or anti-clockwise. The reward is initialized at zero. At each timestep, the reward is equal to minus the current distance (in pixels) between the shape’s position and the image center minus $10 \times$ the smallest angle (in radians) between the shape’s orientation and the null angle. The episode ends when the shape reaches the goal state, with no additional reward.

5 Results

The performance (average episode return) of policies trained (via the PPO algorithm) using latent representations from different models (GW and its baselines) and in different test settings is shown

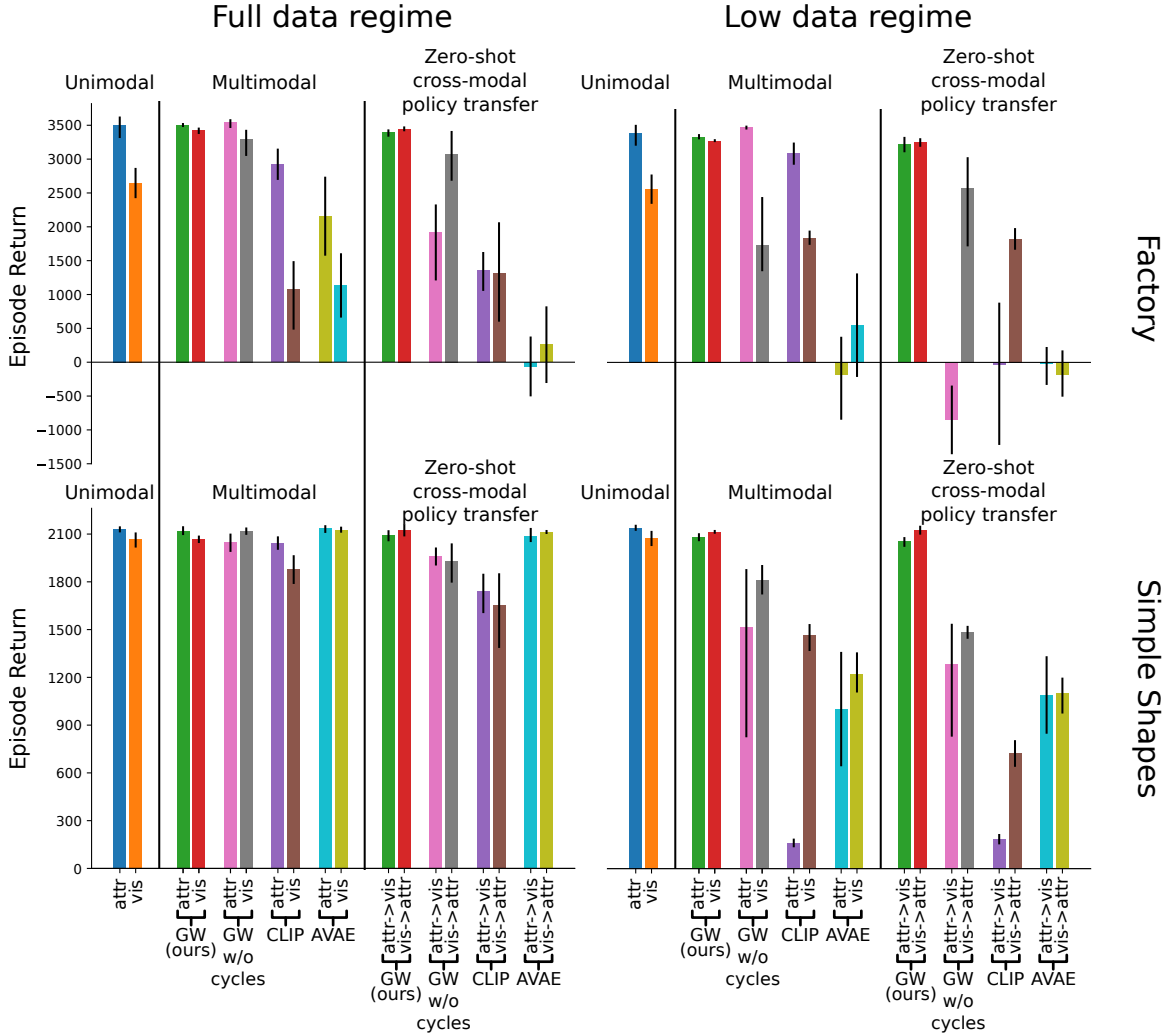


Figure 3: Performance (average episode return) of PPO trained using different latent representations and tested in different settings. A fixed value was subtracted from the episode return, corresponding to the performance of a fully-random policy in each environment; thus the random policy performance (chance level) is equal to zero in all plots (negative values reflect a defective strategy, e.g. systematically hitting walls and receiving penalties). All results are averaged across five different runs (different random seeds for policy training), and the error bars reflect 95% confidence intervals computed via bootstrapping. Models trained in the *Factory* environment are plotted in the top row, and in the bottom row for the *Simple Shapes* environment. Multimodal networks trained with all paired data are plotted in the left column (Full data regime); in the right column, the networks only have access to a subset of multimodal paired data (Low data regime). Each plot is divided into three parts: PPO trained directly from a *unimodal* latent representation; PPO trained and tested on the same *multimodal* latent representation; PPO trained on one multimodal latent representation and tested on the other (*zero-shot cross modal policy transfer*). In any given plot, bars sharing the same color depict the same trained model, tested in different settings.

in Figure 3. Results for the *Factory* environment are shown in the top panels, and in the bottom panels for the *Simple Shapes* environment. In each case, models trained with a Full data regime are plotted on the left, and with a Low data regime on the right.

We first focus on the performance of PPO trained directly on *unimodal* representations, visible on the left part of each plot in Figure 3. As expected, *unimodal* PPO acts as an upper baseline in the *Simple Shapes* environment, which is fully observable from each input modality. This is not the case in *Factory*, where PPO trained from attributes performs better than from vision; this highlights the asymmetry between visual inputs (partial observation) and attributes (entire state observation) in this environment.

The performance of PPO trained and tested on *multimodal* latent representations obtained in a Full data regime are reported in the middle part of the two left plots in Figure 3. In both environments, GW and GW without cycles yield similar rewards as the upper baseline (PPO trained directly from attributes). AVAE achieves similar performance in *Simple Shapes*, but degraded performance in *Factory*. Finally, the CLIP-like model performs poorly in both environments. We can also highlight that in *Factory*, policies trained from GW and (to some extent) GW w/o cycles are able to bridge the performance asymmetry between vision and attribute inputs. This is an example of *multimodal grounding* in the GW, whereby the learned multimodal latent representation of visual inputs is richer and more informative for a downstream decision task than the unimodal visual latent representation. The difference with results from the CLIP-like model reveals the importance of adding broadcast objectives in addition to contrastive alignment.

In the Full data regime scenario, both supervised and semi-supervised GW models (with and without cycles) perform near-optimally when trained and tested on the same *multimodal* latent representations. However, the GW cycles are particularly important when we consider the Low data regime scenario (middle part of the plots on the right in Figure 3). Here, we actually observe a drop in PPO performance for all the models in at least one input modality, except for the full GW. The decreased performance of GW w/o cycles highlights the crucial role played by the unsupervised cycle-consistency objectives in maintaining broadcast and alignment properties when the amount of multimodal paired data is low.

Finally, the zero-shot cross-modal policy transfer capabilities are shown on the right part of each plot of Figure 3. In both the full and low data regimes, and for both environments, the full GW allows for nearly optimal zero-shot transfer between modalities: a policy trained and tested on GW latent representations of attributes performs equally well when tested on GW latent representations of images (green bars), and vice-versa (red bars). The AVAE model is the only other model that permits a similar zero-shot transfer, but only in one of the four experimental settings—*Simple Shapes* in the Full data regime. In the Low data regime of *Simple Shapes* and in both regimes of *Factory*, the policy trained in one AVAE modality does not transfer well to the other. This is also the case for the CLIP-like baseline and for the GW w/o cycles ablation, in all four experimental settings.

In summary, policies learned from a GW latent representation are particularly efficient, and in some cases (e.g., *Factory*) can even surpass policies trained from unimodal representations. In addition, only policies trained from GW latents could systematically generalize to the opposite modality (zero-shot cross-modal transfer). We found that relying only on a contrastive alignment objective to establish a multimodal space (like CLIP) was insufficient. The introduction of broadcast objectives (supported by the GW decoders, see Figure 2) compels the GW encoders to retain most information present in the original unimodal latents, so that they can be accurately reconstructed by the broadcast operation. Such a GW can be trained in a purely supervised way (GW w/o cycles) when both modalities provide fully-observable information (*Simple Shapes*) and when large amounts of paired multimodal data are available for supervised training (Full data regime). In all other scenarios, the inclusion of unsupervised cycle-consistency objectives (full GW model) proves beneficial in preserving information and maintaining alignment between multimodal representations.

6 Conclusion

Our study applied a multimodal representation learning approach previously proposed by Devillers et al. (2023) (an adaptation of the Global Workspace Theory from Cognitive Science) to the training of an RL agent. The implemented model enables the construction of a multimodal latent space,

allowing the encoding of unimodal information and exploiting the synergies between the different modalities. We demonstrated the capability of a GW to enable zero-shot cross-modal policy transfer, illustrating the adaptability and generalization of the learned policies across diverse modalities. Additionally, we highlighted the potential advantages of employing a semi-supervised learning framework, as seen in GW with cycle-consistency, especially in scenarios where data collection can be costly. Using a GW to generate multimodal representations, instead of other existing methods such as CLIP (Radford et al., 2021) or AVAE (Silva et al., 2020), was found to improve policy performance as well as zero-shot policy transfer across modalities. This approach not only showcases the potential of the Global Workspace Theory in enhancing the performance of RL agents, but also opens avenues for the development of more robust and versatile artificial intelligence systems capable of seamlessly transferring knowledge between different sensory domains.

References

- Bernard J. Baars. *A Cognitive Theory of Consciousness*. Cambridge University Press, New York, 1988.
- Stanislas Dehaene, Michel Kerszberg, and Jean-Pierre Changeux. A neuronal model of a global workspace in effortful cognitive tasks. *Proceedings of the National Academy of Sciences*, 95(24): 14529–14534, November 1998. doi: 10.1073/pnas.95.24.14529. URL <https://www.pnas.org/doi/full/10.1073/pnas.95.24.14529>. Publisher: Proceedings of the National Academy of Sciences.
- Benjamin Devillers, Bhavin Choksi, Romain Bielański, and Rufin VanRullen. Does language help generalization in vision models? In Arianna Bisazza and Omri Abend (eds.), *Proceedings of the 25th Conference on Computational Natural Language Learning*, pp. 171–182, Online, November 2021. Association for Computational Linguistics. doi: 10.18653/v1/2021.conll-1.13. URL <https://aclanthology.org/2021.conll-1.13>.
- Benjamin Devillers, Léopold Maytié, and Rufin VanRullen. Semi-supervised Multimodal Representation Learning through a Global Workspace, June 2023. URL <http://arxiv.org/abs/2306.15711>. arXiv:2306.15711 [cs, q-bio].
- Yilun Du, Chuang Gan, and Phillip Isola. Curious Representation Learning for Embodied Intelligence. pp. 10408–10417, 2021. URL https://openaccess.thecvf.com/content/ICCV2021/html/Du_Curious_Representation_Learning_for_Embodied_Intelligence_ICCV_2021_paper.html.
- Chelsea Finn, Xin Yu Tan, Yan Duan, Trevor Darrell, Sergey Levine, and Pieter Abbeel. Deep spatial autoencoders for visuomotor learning. In *2016 IEEE International Conference on Robotics and Automation (ICRA)*, pp. 512–519. IEEE, 2016.
- David Friede, Christian Reimers, Heiner Stuckenschmidt, and Mathias Niepert. Learning Disentangled Discrete Representations. In Danai Koutra, Claudia Plant, Manuel Gomez Rodriguez, Elena Baralis, and Francesco Bonchi (eds.), *Machine Learning and Knowledge Discovery in Databases: Research Track*, Lecture Notes in Computer Science, pp. 593–609, Cham, 2023. Springer Nature Switzerland. ISBN 978-3-031-43421-1. doi: 10.1007/978-3-031-43421-1_35.
- Abhishek Gupta, Coline Devin, YuXuan Liu, Pieter Abbeel, and Sergey Levine. Learning Invariant Feature Spaces to Transfer Skills with Reinforcement Learning, March 2017. URL <http://arxiv.org/abs/1703.02949>. arXiv:1703.02949 [cs].
- David Ha and Jürgen Schmidhuber. World Models. March 2018. doi: 10.5281/zenodo.1207631. URL <http://arxiv.org/abs/1803.10122>. arXiv:1803.10122 [cs, stat].
- Danijar Hafner, Jurgis Pasukonis, Jimmy Ba, and Timothy P. Lillicrap. Mastering Diverse Domains through World Models. *CoRR*, abs/2301.04104, 2023. URL <https://doi.org/10.48550/arXiv.2301.04104>.

-
- Irina Higgins, Arka Pal, Andrei Rusu, Loic Matthey, Christopher Burgess, Alexander Pritzel, Matthew Botvinick, Charles Blundell, and Alexander Lerchner. DARLA: improving zero-shot transfer in reinforcement learning. In *Proceedings of the 34th International Conference on Machine Learning - Volume 70*, ICML'17, pp. 1480–1490, Sydney, NSW, Australia, August 2017. JMLR.org.
- Douwe Kiela and Stephen Clark. Multi- and Cross-Modal Semantics Beyond Vision: Grounding in Auditory Perception. In Lluís Màrquez, Chris Callison-Burch, and Jian Su (eds.), *Proceedings of the 2015 Conference on Empirical Methods in Natural Language Processing*, pp. 2461–2470, Lisbon, Portugal, September 2015. Association for Computational Linguistics. doi: 10.18653/v1/D15-1293. URL <https://aclanthology.org/D15-1293>.
- Michael Laskin, Aravind Srinivas, and Pieter Abbeel. CURL: Contrastive Unsupervised Representations for Reinforcement Learning. In *Proceedings of the 37th International Conference on Machine Learning*, pp. 5639–5650. PMLR, November 2020. URL <https://proceedings.mlr.press/v119/laskin20a.html>. ISSN: 2640-3498.
- Michelle A. Lee, Yuke Zhu, Krishnan Srinivasan, Parth Shah, Silvio Savarese, Li Fei-Fei, Animesh Garg, and Jeannette Bohg. Making Sense of Vision and Touch: Self-Supervised Learning of Multimodal Representations for Contact-Rich Tasks. In *2019 International Conference on Robotics and Automation (ICRA)*, pp. 8943–8950, May 2019. doi: 10.1109/ICRA.2019.8793485. URL <https://ieeexplore.ieee.org/document/8793485>. ISSN: 2577-087X.
- Volodymyr Mnih, Adria Puigdomenech Badia, Mehdi Mirza, Alex Graves, Timothy Lillicrap, Tim Harley, David Silver, and Koray Kavukcuoglu. Asynchronous Methods for Deep Reinforcement Learning. In *Proceedings of The 33rd International Conference on Machine Learning*, pp. 1928–1937. PMLR, June 2016. URL <https://proceedings.mlr.press/v48/mniha16.html>. ISSN: 1938-7228.
- Hai Pham, Paul Pu Liang, Thomas Manzini, Louis-Philippe Morency, and Barnabás Póczos. Found in Translation: Learning Robust Joint Representations by Cyclic Translations between Modalities. *Proceedings of the AAAI Conference on Artificial Intelligence*, 33(01):6892–6899, July 2019. ISSN 2374-3468. doi: 10.1609/aaai.v33i01.33016892. URL <https://ojs.aaai.org/index.php/AAAI/article/view/4666>. Number: 01.
- Alec Radford, Jong Wook Kim, Chris Hallacy, Aditya Ramesh, Gabriel Goh, Sandhini Agarwal, Girish Sastry, Amanda Askell, Pamela Mishkin, Jack Clark, Gretchen Krueger, and Ilya Sutskever. Learning Transferable Visual Models From Natural Language Supervision. In *Proceedings of the 38th International Conference on Machine Learning*, pp. 8748–8763. PMLR, July 2021. URL <https://proceedings.mlr.press/v139/radford21a.html>. ISSN: 2640-3498.
- John Schulman, Filip Wolski, Prafulla Dhariwal, Alec Radford, and Oleg Klimov. Proximal Policy Optimization Algorithms, August 2017. URL <http://arxiv.org/abs/1707.06347>. arXiv:1707.06347 [cs].
- Carina Silberer and Mirella Lapata. Grounded Models of Semantic Representation. In Jun’ichi Tsujii, James Henderson, and Marius Pasca (eds.), *Proceedings of the 2012 Joint Conference on Empirical Methods in Natural Language Processing and Computational Natural Language Learning*, pp. 1423–1433, Jeju Island, Korea, July 2012. Association for Computational Linguistics. URL <https://aclanthology.org/D12-1130>.
- Rui Silva, Miguel Vasco, Francisco S Melo, Ana Paiva, and Manuela Veloso. Playing Games in the Dark: An Approach for Cross-Modality Transfer in Reinforcement Learning. *Proceedings of the 19th International Conference on Autonomous Agents and MultiAgent Systems (AAMAS)*, pp. 1260–1268, 2020.

-
- Kunal Pratap Singh, Jordi Salvador, Luca Weihs, and Aniruddha Kembhavi. Scene Graph Contrastive Learning for Embodied Navigation. In *2023 IEEE/CVF International Conference on Computer Vision (ICCV)*, pp. 10850–10860, Paris, France, October 2023. IEEE. ISBN 9798350307184. doi: 10.1109/ICCV51070.2023.00999. URL <https://ieeexplore.ieee.org/document/10377327/>.
- R.S. Sutton and A.G. Barto. Reinforcement learning: An introduction. *IEEE Transactions on Neural Networks*, 9(5):1054–1054, 1998. doi: 10.1109/TNN.1998.712192.
- Mark Towers, Jordan K. Terry, Ariel Kwiatkowski, John U. Balis, Gianluca de Cola, Tristan Deleu, Manuel Goulão, Andreas Kallinteris, Arjun KG, Markus Krimmel, Rodrigo Perez-Vicente, Andrea Pierré, Sander Schulhoff, Jun Jet Tai, Andrew Tan Jin Shen, and Omar G. Younis. Gymnasium, March 2023. URL <https://zenodo.org/record/8127025>.
- Rufin VanRullen and Ryota Kanai. Deep learning and the Global Workspace Theory. *Trends in Neurosciences*, 44(9):692–704, September 2021. ISSN 0166-2236, 1878-108X. doi: 10.1016/j.tins.2021.04.005. URL [https://www.cell.com/trends/neurosciences/abstract/S0166-2236\(21\)00077-1](https://www.cell.com/trends/neurosciences/abstract/S0166-2236(21)00077-1). Publisher: Elsevier.
- Xin Wang, Hong Chen, Yuwei Zhou, Jianxin Ma, and Wenwu Zhu. Disentangled Representation Learning for Recommendation. *IEEE Transactions on Pattern Analysis and Machine Intelligence*, 45(1):408–424, January 2023. ISSN 1939-3539. doi: 10.1109/TPAMI.2022.3153112. URL <https://ieeexplore.ieee.org/abstract/document/9720218>. Conference Name: IEEE Transactions on Pattern Analysis and Machine Intelligence.
- Manuel Watter, Jost Springenberg, Joschka Boedecker, and Martin Riedmiller. Embed to Control: A Locally Linear Latent Dynamics Model for Control from Raw Images. In *Advances in Neural Information Processing Systems*, volume 28. Curran Associates, Inc., 2015. URL https://proceedings.neurips.cc/paper_files/paper/2015/hash/a1afc58c6ca9540d057299ec3016d726-Abstract.html.
- Webots. <http://www.cyberbotics.com>. URL <http://www.cyberbotics.com>.
- Hang Yin, Francisco Melo, Aude Billard, and Ana Paiva. Associate Latent Encodings in Learning from Demonstrations. *Proceedings of the AAAI Conference on Artificial Intelligence*, 31(1), February 2017. ISSN 2374-3468. doi: 10.1609/aaai.v31i1.11040. URL <https://ojs.aaai.org/index.php/AAAI/article/view/11040>. Number: 1.

A Model Parameters

In this Appendix, we provide details about our models’ implementation, starting with the VAE used in both visual environments: *Simple Shapes* (Table 1) and *Factory* (Table 2). In the VAE encoder, all convolutions have a padding of 1, a stride of 2, and a kernel-size of 4. For the decoders, in *Simple Shapes* (Table 1), the transposed convolutions have a padding of 1, a stride of 2, and a kernel size of 4, except the first one which has a stride of 1. The final convolution has a stride of 1 and a kernel size of 4. In *Factory* (Table 2), the transposed convolutions have a padding of 2, a stride of 2, and a kernel size of 5, except the first one which has a stride of 1 and a kernel size of 8 without padding. The final convolution has a stride of 1 and a kernel size of 5.

VAE encoder (2.8M params)	VAE decoder (3M params)
$x \in \mathbb{R}^{3 \times 32 \times 32}$	$z \in \mathbb{R}^{12}$
Conv ₁₂₈ – BN – ReLU	FC _{8×8×1024}
Conv ₂₅₆ – BN – ReLU	ConvT ₅₁₂ – BN – ReLU
Conv ₅₁₂ – BN – ReLU	ConvT ₂₅₆ – BN – ReLU
Conv ₁₀₂₄ – BN – ReLU	ConvT ₁₂₈ – BN – ReLU
Flatten – FC _{2×12}	Conv ₁ – Sigmoid

Table 1: Architecture and number of parameters of the VAE used in the *Simple Shapes* environment.

VAE encoder (2.8M params)	VAE decoder (5M params)
$x \in \mathbb{R}^{3 \times 128 \times 128}$	$z \in \mathbb{R}^{10}$
Conv ₁₂₈ – BN – ReLU	FC _{8×8×512}
Conv ₂₅₆ – BN – ReLU	ConvT ₂₅₆ – BN – ReLU
Conv ₅₁₂ – BN – ReLU	ConvT ₁₂₈ – BN – ReLU
Conv ₁₀₂₄ – BN – ReLU	ConvT ₆₄ – BN – ReLU
Flatten – FC ₁₀	Conv ₁ – Sigmoid

Table 2: Architecture and number of parameters of the VAE used in the *Factory* environment.

Table 3 and Table 4 present details about the Global Workspace architecture for respectively *Simple Shapes* and *Factory*. The tables show the architecture for the encoder and decoder of only one modality, since they are nearly identical across modalities. Only the last Fully Connected layer of the decoders is different, outputting a vector of the original size of each domain.

GW encoder (35K params)	GW decoder (50K params)
FC ₁₂₈ – ReLU	FC ₁₂₈ – ReLU
FC ₁₂₈ – ReLU	FC ₁₂₈ – ReLU
FC ₁₂₈ – ReLU	FC ₁₂₈ – ReLU
FC	FC

Table 3: Architecture and number of parameters for the encoder and decoder in the GW of one modality in *Simple Shapes*

The implementation details for AVAE are presented in Table 5 for *Simple Shapes* and Table 6 for *Factory*. In both environments the parameters for the Conv and ConvT layers in the image VAE are the same as the ones used in their respective VAE in Tables 1 and 2. For *Simple Shapes*, the input layer of the attributes side is divided in two Fully Connected layers: one for the category of the shape (one-hot vector) and one for the rest of the attributes (continuous values).

GW encoder (1.3M params)	GW decoder (1.3M params)
FC ₅₁₂ – ReLU	FC ₅₁₂ – ReLU
FC ₅₁₂ – ReLU	FC ₅₁₂ – ReLU
FC ₅₁₂ – ReLU	FC ₅₁₂ – ReLU
FC ₅₁₂ – ReLU	FC ₅₁₂ – ReLU
FC ₅₁₂ – ReLU	FC ₅₁₂ – ReLU
FC	FC

Table 4: Architecture and number of parameters for the encoder and decoder in the GW of one modality in *Factory*

AVAE vision (6M params)	AVAE attributes (0.6M params)
$x \in \mathbb{R}^{3 \times 32 \times 32}$	$x \in \{0, 1\}^3 \times \mathbb{R}^8$
Conv ₁₂₈ – BN – ReLU	FC ₁₂₈ – ReLU
Conv ₂₅₆ – BN – ReLU	FC ₁₂₈ – ReLU
Conv ₅₁₂ – BN – ReLU	FC ₁₂ – ReLU
Conv ₁₀₂₄ – BN – ReLU	
Flatten – FC _{2×12}	FC _{2×12}
$z \in \mathbb{R}^{12}$	$z \in \mathbb{R}^{12}$
FC _{8×8×1024}	
ConvT ₅₁₂ – BN – ReLU	FC ₁₂₈ – ReLU
ConvT ₂₅₆ – BN – ReLU	FC ₁₂₈ – ReLU
ConvT ₁₂₈ – BN – ReLU	[FC ₃ , FC ₈ – Tanh]
Conv ₁ – Sigmoid	

Table 5: Architecture and number of parameters of the visual and attributes VAEs of the AVAE for the *Simple Shapes* environment.

AVAE vision (11M params)	AVAE attributes (2M params)
$x \in \mathbb{R}^{3 \times 128 \times 128}$	$x \in \mathbb{R}^{10}$
Conv ₁₂₈ – BN – ReLU	FC ₅₁₂ – ReLU
Conv ₂₅₆ – BN – ReLU	FC ₅₁₂ – ReLU
Conv ₅₁₂ – BN – ReLU	FC ₄₀ – ReLU
Conv ₁₀₂₄ – BN – ReLU	
Flatten – FC _{2×40}	FC _{2×40}
$z \in \mathbb{R}^{40}$	$z \in \mathbb{R}^{40}$
FC _{8×8×1024}	
ConvT ₅₁₂ – BN – ReLU	FC ₅₁₂ – ReLU
ConvT ₂₅₆ – BN – ReLU	FC ₅₁₂ – ReLU
ConvT ₁₂₈ – BN – ReLU	FC ₁₀ – Tanh
Conv ₁ – Sigmoid	

Table 6: Architecture and number of parameters of the visual and attributes VAEs of the AVAE for the *Factory* environment.

B GW losses details

As explained in 3, the Global Workspace (GW) is trained with four different losses. Here we provide details of their implementation, following [Devillers et al. \(2023\)](#).

$$\begin{aligned}
L_{tr} &= \frac{1}{2}[L_{attr}(d_{attr}(e_v(o_v^i)), o_{attr}^j) + L_v(d_v(e_{attr}(o_{attr}^j)), o_v^i)] \\
L_{cont} &= CONT[e_v(o_v^i), e_{attr}(o_{attr}^j)] \\
L_{dcy} &= \frac{1}{2}[L_v(d_v(e_v(o_v^i)), o_v^i) + L_{attr}(d_{attr}(e_{attr}(o_{attr}^j)), o_{attr}^j)] \\
L_{cy} &= \frac{1}{2}[L_v(d_v(e_{attr}(d_{attr}(e_v(o_v^i))))), o_v^i) + L_{attr}(d_{attr}(e_v(d_v(e_{attr}(o_{attr}^j))))), o_{attr}^j)]
\end{aligned}$$

Where $CONT()$ is the contrastive loss used in the CLIP model (Radford et al., 2021). L_{attr} represents the reconstruction loss used on the attributes side, which differs between the two environments. In *Factory* (where all attributes have continuous values), it is computed with an MSE; in *Simple Shapes* it is a combination of a negative log-likelihood for shape classes (discrete one-hot encoded values) and MSE for the other (continuous) attributes. L_v represents the reconstruction loss on the visual side, computed with an MSE in both environments. The total loss is then computed as follows :

$$L_{GW} = \alpha \cdot L_{tr} + \beta \cdot L_{cont} + \gamma \cdot L_{dcy} + \theta \cdot L_{cy}$$

Where $\alpha, \beta, \gamma, \theta$ are hyperparameters giving more or less importance to each loss. The following table contains the hyperparameters for all Global Workspace models (and ablations) in the Full data regime in both environments.

	GW	GW w/o cycles	CLIP-like
Factory	$\alpha = 1$	$\alpha = 1$	$\alpha = 0$
	$\beta = 0.1$	$\beta = 0.1$	$\beta = 1$
	$\gamma = 1$	$\gamma = 0$	$\gamma = 0$
	$\theta = 1$	$\theta = 0$	$\theta = 0$
Simple Shapes	$\alpha = 1$	$\alpha = 1$	$\alpha = 0$
	$\beta = 0.1$	$\beta = 0.1$	$\beta = 1$
	$\gamma = 5$	$\gamma = 0$	$\gamma = 0$
	$\theta = 5$	$\theta = 0$	$\theta = 0$

The table below shows the hyperparameters used in the Low data regime in both environments.

	GW	GW w/o cycles	CLIP-like
Factory	$\alpha = 1$	$\alpha = 1$	$\alpha = 0$
	$\beta = 0.1$	$\beta = 0.1$	$\beta = 1$
	$\gamma = 5$	$\gamma = 0$	$\gamma = 0$
	$\theta = 5$	$\theta = 0$	$\theta = 0$
Simple Shapes	$\alpha = 1$	$\alpha = 1$	$\alpha = 0$
	$\beta = 0.1$	$\beta = 0.1$	$\beta = 1$
	$\gamma = 10$	$\gamma = 0$	$\gamma = 0$
	$\theta = 10$	$\theta = 0$	$\theta = 0$

C Reward details

The reward in the *Factory* environment is given by a combination of the distance between the robot and the table, and the angle between the orientation of the robot and the table (this is meant to encourage the policy to turn the robot facing the table, regardless of its original location):

$$\begin{aligned}
r &= -\text{distance} - 10 \times \text{angle} \\
r &= -\sqrt{(x_r - x_t)^2 + (y_r - y_t)^2} - 10 \times \left| \arccos([c_{\theta_r}, s_{\theta_r}], \frac{[x_t - x_r, y_t - y_r]}{\|[x_t - x_r, y_t - y_r]\|_2}) \right|
\end{aligned}$$

The reward in the *Simple Shapes* environment is given by a combination of the distance between the position of the shape and the center of the image, and the angle of the shape:

$$r = -\text{distance} - 10 \times \text{angle}$$

$$r = -\sqrt{(x - 16)^2 + (y - 16)^2} - 10 \times |\arccos([c_\theta, s_\theta], [1, 0])|$$

D A2C in Simple Shapes scenario

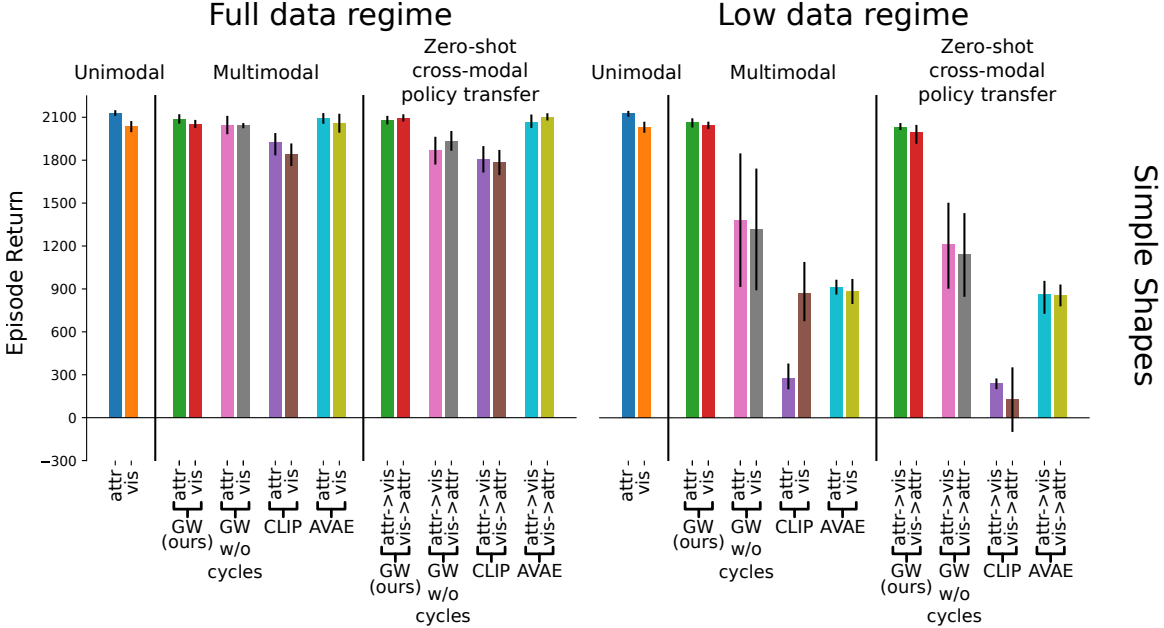


Figure 4: Performance of A2C in the Simple Shapes environment. Notations and conventions as in Figure 3.

An additional experiment was performed in the Simple Shapes environment to verify that our results were robust to the choice of policy training algorithm. For this, we used A2C, introduced by Mnih et al. (2016). Figure 4 shows that the results are reproducible with this alternative algorithm (compare with Figure 3, bottom). A2C trained from a Global Workspace performs as well as when trained on unimodal representations, both in terms of absolute performance and in terms of zero-shot cross-modal transfer. AVAE performs similarly in the Full data regime, but poorly in the Low data regime. The two other models (Global Workspace without cycles and CLIP-like ablation), give worse performance in both regimes, as in the case of PPO.